Available online at www.sciencedirect.com
ScienceDirect
Journal of Organometallic Chemistry 692 (2007) 2046–2055
Journal of Organometallic Chemistry
www.elsevier.com/locate/jorganchem

Electronic interactions in 1-ethynyl-2-phenyltetramethyldisilanes $HC{\equiv}CSiMe_2SiMe_2C_6H_4X$

Jennifer A. Shaw-Taberlet [a], Jean-René Hamon [a], Thiery Roisnel [a], Claude Lapinte [a], Michaela Flock [b], Thomas Mitterfellner [b], Harald Stueger [b,*]

[a] *UMR 6226 Sciences Chimiques de Rennes, CNRS-Université de Rennes 1, Campus de Beaulieu, 35042 Rennes Cedex, France*
[b] *Institut für Anorganische Chemie, Technische Universität Graz, Stremayrgasse 16, A-8010 Graz, Austria*

Received 25 October 2006; received in revised form 10 January 2007; accepted 16 January 2007
Available online 24 January 2007

Abstract

1-Ethynyl-2-phenyltetramethyldisilanes $HC{\equiv}CSiMe_2SiMe_2C_6H_4X$ [X = NMe_2 (**1**), H (**2**), CH_3 (**3**), Br (**4**), CF_3 (**5**)] are accessible from $ClSiMe_2SiMe_2Cl$, $BrMgC_6H_4X$ and $HC{\equiv}CMgBr$ in a two step Grignard reaction. The crystal structure of **1** as determined by single crystal X-ray crystallography exhibits a nearly planar $PhNMe_2$ moiety and an unusual *gauche* array of the phenyl and the acetylene group with respect to rotation around the Si–Si bond. Full geometry optimization (B3LYP/6-31+G**) of the gas phase structures of **1**–**5** affords minima for the *gauche* and the *anti* rotational isomers, both being very close in energy with a rotational barrier of only 3–5 kJ/mol. Experimental and calculated (time-dependent DFT B3LYP/TZVP) UV absorption data of **1**–**5** show pronounced electronic interactions of the $HC{\equiv}C$– and the C_6H_4X π-systems with the central Si–Si bond.

Keywords: UV absorption spectra; Disilanes; Hyperconjugation; DFT calculations

1. Introduction

It is well known that disilanes possess interesting physical properties owing to their σ-electronic system, which is characterized by a HOMO high in energy and a LUMO low in energy [1]. This property is invoked to explain, why σ-bonding electrons are delocalized across a polysilane network in a manner comparable to the delocalization of conjugated organic π-electrons giving Si–Si bonded species quite interesting properties [2] like unusually long wavelength UV absorption maxima, low ionization energies, nonlinear optical behavior [3], fluorescence [4] or photochemical activity. σ-Delocalization in Si–Si bonded compounds has also been treated theoretically on various levels of theory including simple Hueckel, semiempirical, ab initio and DFT methods [5].

In addition, pronounced substituent effects on polysilane properties such as bathochromically shifted UV/visible absorption maxima are observed, when unsaturated organic side groups like phenyl, vinyl or acetylene moieties or atoms with π symmetric lone pairs like the halogens, O or N are linked directly to the Si–Si bond [6]. At first such interactions were rationalized in terms of d–π* hybridization in the excited state. Later, the importance of σ–π conjugation (hyperconjugation) in the ground state between the Si–Si σ-bond and the adjacent π symmetric orbitals were recognized [2a]. Thus, it has been demonstrated by photoelectron spectroscopy, that the HOMO of phenylpentamethyldisilane is a linear combination of Si–Si σ and C_6H_5 π orbitals [1a]. In a related study Sakurai et al. furnished indications of the σ-donating character of the Si–Si bond [7]. Meanwhile it has been generally accepted, that σ–π or σ–*n* conjugation is the key factor for the substituent effects influencing polysilane properties. In $PhMe_2SiSiMe_3$, for instance, σ–π hyperconjugation is responsible for the observed rise of the energy of the highest occupied Si–Si

* Corresponding author. Tel./fax: +43 316 873 8708.
E-mail address: harald.stueger@tugraz.at (H. Stueger).

0022-328X/$ - see front matter © 2007 Elsevier B.V. All rights reserved.
doi:10.1016/j.jorganchem.2007.01.024

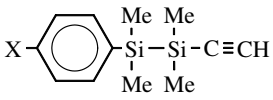

Fig. 1. General structure of the family of σ–π conjugated disilanes reported herein: **1**, X = NMe_2; **2**, X=H; **3**, X=CH_3; **4**, X=Br; **5**, X=CF_3.

σ-level relative to $Me_3SiSiMe_3$ and the concomitant decrease of the UV-excitation energy [1a].

A series of recent investigations revealed, that the UV/vis absorption spectra and other photophysical properties of polysilanes are drastically influenced by the silicon backbone comformation. The topic was comprehensively reviewed lately [8]. It has been widely accepted that the *anti* conformation effectively extends σ-delocalization while the *gauche* form does not. As a consequence, an *all-anti* conformer of a polysilane is supposed to afford a bathochromically shifted first UV absorption maximum. The UV absorption spectra of σ–π conjugated systems also show remarkable conformational dependence. A careful study of the absorption spectra of conformationally constrained aryldisilanes demonstrated that a torsion angle between the phenyl ring plane and the Si–Si bond of 90° effects in maximum σ–π conjugation [9]. Similar conformational dependence of UV absorption and emission properties was also observed, when the 1,2-diphenyldisilane moiety is conformationally constrained by incorporation into cyclic structures [10].

The present contribution describes the synthesis and characterization of several previously unknown conjugated disilanes of the general type shown in Fig. 1. NMR and UV/vis spectroscopic data are used together with the results of an X-ray crystal structure determination of **1** to study the degree of electron delocalization in **1**–**5** and to detect possible interactions of the phenyl and acetylene π-systems via the silicon–silicon bond. Furthermore, experimental data are rationalized by appropriate DFT calculations.

2. Results and discussion

2.1. Preparation

Novel disilanyl acetylides **1**, **3**, **4** and **5** were synthesized in three steps from tetramethyldichlorodisilane via well known methods, adapted to each reaction [11]. The general procedure is illustrated in Scheme 1. The first step involves the *in situ* formation of the *para* substituted phenyl Grignard reagent, which displaces a chlorine atom in $ClSiMe_2SiMe_2Cl$ by nucleophilic substitution. The resulting chlorosilane intermediates were partially characterized, the corresponding data can be found in the experimental section. The second chlorine atom of these intermediates was then displaced by ethynyl magnesium bromide.

The yields after purification were moderate to good. For liquid compounds **3**, **4** and **5**, the workup consisted of extraction of the crude mixture with pentane, followed by distillation and gave the desired product at a spectroscopic purity level. The Me_2N-derivative **1**, a salt-like white solid at room temperature, was crystallized from a concentrated pentane solution at −40 °C after distillation. The clear, colorless crystals obtained were stored at −70 °C due to their tendency to change color to brown upon standing at room temperature. It is interesting to note that such color changes were not accompanied by changes in the spectroscopic data. Generally all products were characterized by standard spectroscopic techniques (^{29}Si, ^{13}C and ^{1}H NMR, IR, HRMS). The results (compare experimental section) agree well with the proposed structures in all cases.

2.2. NMR Spectroscopy

Only weak electronic effects of the substituents attached to the aromatic ring are apparent in the ^{29}Si NMR spectra. Thus, compounds **1**–**5**, exhibit very similar ^{29}Si chemical shift values for the silicon atom α to the phenyl ring within the close range of only 2 ppm. The same is true for the ^{13}C chemical shifts of the acetylene carbons, which are nearly unaffected by the presence of electron withdrawing or electron donating substituents attached to the phenyl ring. Substituent effects as expected for *p*-disubstituted benzene derivatives, however, are found for the ^{13}C resonance lines of the aromatic carbon atoms. A simple empirical method based on substituent increments Z_i can be used to predict benzene ring ^{13}C shifts according to following equations [12]:

$$Z_i = \delta_i(C_6H_5X) - 128.5(\text{ppm}) \quad (1)$$

$$\delta_{i(C_6H_{6-n}X_n)} = 128.5 + \sum Z_i(\text{ppm}) \quad (2)$$

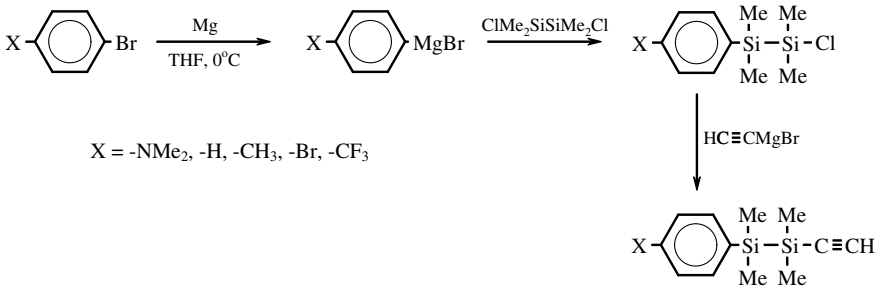

Scheme 1.

Originating from monosubstituted benzenes, however, these shift increments do not take into account interactions between multiple phenyl substituents. Deviation of experimental and predicted values, therefore, are to be expected, if substituents show interactions like strong resonance or inductive effects of opposite signs. Experimental and predicted ^{13}C chemical shift values of the aromatic carbons in **1**–**5** are collected in Table 1. Excellent correlation between experimental and calculated values is observed for **3** containing the weakly donating methyl group (maximum deviation, 1 ppm), while **1**, **4** and **5** exhibit somewhat larger deviations of different magnitude and sign pointing towards enhanced interaction of the disilanyl moiety with the *p*-NMe_2, Br and CF_3 substituents, respectively.

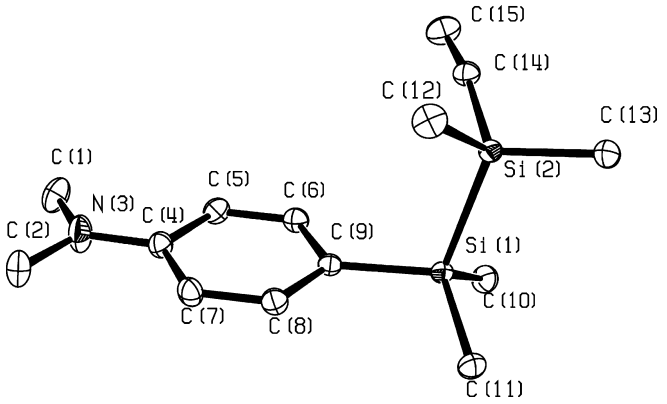

Fig. 2. ORTEP drawing and numbering of **1**. Thermal ellipsoids are shown at the 50% probability level. Hydrogen atoms have been omitted for clarity.

2.3. Molecular structure of *1*

The molecular structure of **1** was determined by X-ray crystallography on a monocrystal. The data are summarized along with DFT calculated values in Table 2. An ORTEP diagram can be found in Fig. 2.

With a sum of the C–N–C angles being 359.8° the Me_2N-moiety is nearly perfectly planar. Furthermore, this substituent crystallizes nearly coplanar to the phenyl ring as shown by the C2–N3–C4–C5 dihedral angle of 178.2°. The N3–C4 bond with a bond length of 137.5 pm is significantly shorter as compared to the C1–N3 and C2–N3 single bonds (144.2 and 144.4 pm). Both facts indicate a strong degree of resonance delocalization from the nitrogen lone

Table 1
Experimental and calculated ^{13}C chemical shifts of **1**–**5**

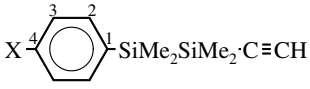

X	δC_1		δC_2		δC_3		δC_4	
	Exp.[a]	Calc.[b]	Exp.[a]	Calc.[b]	Exp.[a]	Calc.[b]	Exp.[a]	Calc.[b]
–H[c]	138.0		134.0		128.0		128.9	
$–NMe_2$	122.6	126.2	135.1	134.2	112.2	113.1	150.9	150.0
$–CH_3$	134.2	135.0	134.1	134.7	128.8	127.8	138.6	138.2
–Br	136.9	136.5	135.5	135.5	131.0	130.9	125.7	123.0
$–CF_3$	143.5	141.3	134.3	134.3	124.8	124.8	127.2	131.2

[a] Signal assignment is based on decoupled experiments.
[b] Data calculated by Eq. (2). Values for Z_i are taken from Ref. [11b].
[c] Experimental spectrum recorded in order to calculate Z_i using Eq. (1).

Table 2
Experimental and calculated bond lengths, angles and torsion angles for *gauche*-**1**

Bond length (pm)	Exp.	Calc.	Bond angle (°)	Exp.	Calc.
Si1–Si2	233.64(4)	237.48	C1–N3–C2	119.22(10)	117.0
Si1–C9	187.02(10)	188.79	C1–N3–C4	120.24(10)	119.1
Si2–C14	184.98(11)	185.27	C2–N3–C4	120.37(10)	119.0
$Si–C_{methyl}$ (mean)	187.1		Si2–C14–C15	172.20(11)	178.8
C14–C15	119.10(16)	121.86	$C4_{(Ph\ centroid)}$–C9–Si1	176.90	179.1
C4–C5	140.83(15)	141.54			
C5–C6	138.39(15)	139.25	Torsion angle (°)		
C6–C9	140.00(14)	140.87	C2–N3–C4–C7	1.14	13.3
C9–C8	140.11(14)	140.70	C1–N3–C4–C5	6.60	−12.8
C8–C7	138.58(15)	139.41	C9–Si1–Si2–C14	−66.92	−71.7
C7–C4	140.75(15)	141.43	C8–C9–Si1–Si2	−97.14	−107.3
C1–N3	144.23(15)	145.53	C6–C9–Si1–Si2	79.24	72.1
C2–N3	144.41(15)	145.52			
N3–C4	137.54(14)	139.25			

pair across the aromatic ring. Accordingly we observe some quasi-quinoidal character of the phenyl ring as evidenced by slightly shortened C5–C6 and C7–C8 bond lengths, although the difference is not large enough to allow more definite conclusions.

Si–Si and Si–C bond lengths measure at the expected values for single bonds. The geometry around the silicon atoms is approximately tetrahedral. Interestingly, the bond angle formed between the ethynyl triple bond and Si2 deviates from linearity (172.20°), which could be rationalized by hyperconjugational type σ–π interactions within the C≡C–Si–Si moiety of **1**. In a similar fashion the phenyl plane is bent towards to the Si1–Si2 σ bond as evidenced by the $C_{Ph\ centroid}$–C9–Si1 bond angle of 176.90°.

Compound **1** exhibits an unusual *gauche*-array of the phenyl relative to the acetylene group (C9–Si1–Si2–C14 = 66.9°), while 1,2-diaryldisilanes usually adopt an *anti*-geometry of the central X–Si–Si–X moiety [3b,13]. Theoretical calculations (see below) suggest that the *gauche* conformation observed for **1** in the crystalline state could be favored due to packing, rather than electronic effects. The roughly perpendicular arrangement of the plane of the phenyl ring relative to the Si–Si bond with a dihedral angle C8–C9–Si1–Si2 of 97.14° allows effective overlap for σ–π conjugation between these groups.

Full geometry optimization (B3LYP/6-31+G**) of the gas phase molecular structures of **1**–**5** affords two minima very close in energy, which can be considered as rotational isomers with respect to rotation around the silicon–silicon bond. The calculated structures for compound **1** are illustrated in Fig. 3. In all cases the *gauche* isomer is slightly less stable than the *anti* isomer with an energy differences between 1.34 kJ/mol (**5**) and 1.63 kJ/mol (**1**). In order to estimate the rotational barrier between the two conformers, a series of calculations has been performed for **1**, in which the C_{sp}–Si–Si–C_{sp2} dihedral angle α was varied from 0° to 180° (see Fig. 4). Minima were found at α = −178.9° (*anti*) and 71.7° (*gauche*) with rotational barriers of 3 kJ/mol for *anti* → *gauche* and 5 kJ/mol for *gauche* → *anti*. The small rotational barrier and the negligible energy difference between the *gauche* and the *anti* form indicate nearly unhindered rotation around the Si–Si bond and equal population of both rotamers in the gas phase at room temperature.

Bond lengths, bond angles and dihedral angles calculated for **1**–**5** do not show significant variations with the substituents attached to the phenyl ring. The corresponding data can be found in the Supplementary material. Agreement between the calculated and the experimental

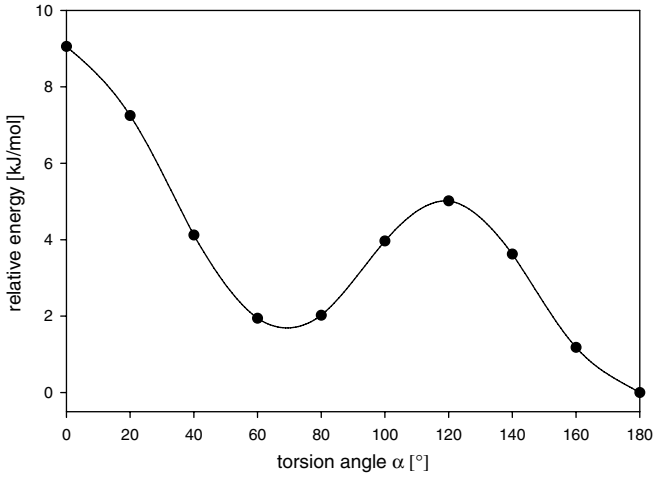

Fig. 4. Variation of the relative energy of **1** as the dihedral angle α (C9–Si1–Si2–C14) is varied from 0° to 180°.

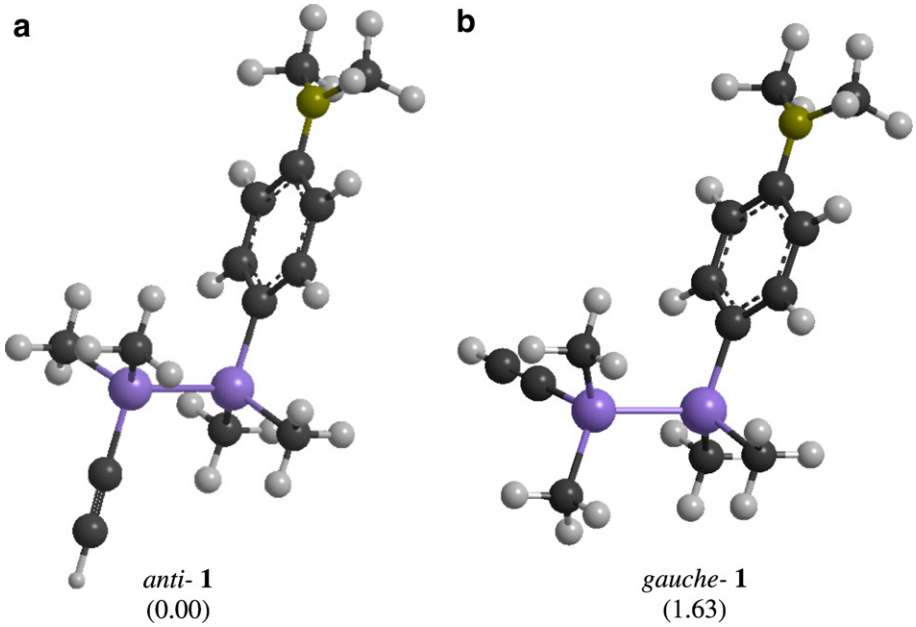

Fig. 3. DFT (B3LYP/6-31+G**) optimized geometries and relative energies for **1**.

molecular structure of **1** is reasonably good (compare Table 2), although the calculations were carried out for the gas phase. A weak quinoidal character of the phenyl ring is also observed computationally, which clearly reflects the influence of the Me_2N– donor on the aromatic system. However, many structural indications of electronic conjugation found experimentally are less pronounced in the theoretical model. Thus, the environment of the N atom is calculated to be slightly pyramidal with a sum of the C–N–C bond angles of 354.6° (*anti*) and 355.1° (*gauche*), respectively. Furthermore, the torsion angles between the planes formed by the Me_2N-group and the phenyl ring are much larger in the calculated structure, while the calculated torsion angles formed between the phenyl plane and the disilyl substituent deviate much more from the ideal 90° than the experimental value. The deviation of the Si2–C≡C bond angle from linearity and the bending of the plane of the phenyl ring towards the Si–Si bond axis are not reflected by the quantum chemical calculations at all. Because the computational method used in the present study usually reflects structural features arising from σ–π delocalization quite well, the observed discrepancy of calculated and experimental structures are most likely due to crystal packing effects and intermolecular interactions occurring exclusively in the solid state.

2.4. UV/vis absorption spectra

UV absorption data of **1**–**5** are presented in Table 3 together with calculated values (Turbomole 5.6 B3LYP/TZVP) and literature data for the corresponding Me_5Si_2-derivatives.

All compounds exhibit absorption maxima in the near UV region. The impact of the HC≡C-group on the absorption characteristics is negligibly small as can be easily judged by comparing the λ_{max} and absorptivity values obtained for **1**–**5** with the corresponding data of their Me_5Si_2-analogues.

Two basic types of absorption spectra are observed within the series **1**–**5**. The absorption spectra of **2**–**5** are surprisingly similar with λ_{max} values between 233 and 239 nm and slightly red shifted first absorption bands for the Br- and CF_3 derivatives **4** and **5** relative to **2** and **3**. The Me_2N– substituted compound **1**, however, exhibits a first absorption maximum at 271 nm with unusually high intensity, the position of which is much less affected by the nature of the organosilicon substituent attached to the benzene ring. Thus, going from Me_2N–C_6H_4–$SiMe_3$ ($\lambda_{max} = 266$ nm) [14] to **1**, a bathochromic shift of just 5 nm is observed, while the first absorption maximum of compound **2**, for instance, is shifted to the red by 22 nm as compared to $PhSiMe_3$ ($\lambda_{max} = 211$ nm) [4a].

In order to achieve a tentative assignment of the low energy absorption bands the absorption spectra of **1**–**5** were calculated by time-dependent DFT at the B3LYP/TZVP level. The features apparent in spectra of **2**–**5** can be interpreted straightforwardly assuming σ–π conjugation between the Si–Si σ-orbital and the π systems of the unsaturated substituents as described in the introductory section. A qualitative molecular orbital diagram for **2** is depicted in Fig. 5 together with the shape of the calculated frontier orbitals (B3LYP/6-31+G**).

Upon UV irradiation an electron is excited from the HOMO, which is delocalized over the whole Ph–Si–Si–C≡C framework, to a LUMO of predominant π*(Ph) character. Because the highest occupied π-MO's of the Ph–X and C≡C substituents in **3**, **4** and **5** are also found well below the highest σ(Si–Si) level as shown by the first ionization potentials estimated by photoelectron spectroscopy ($C_6H_5CH_3$: $IP_1 = -8.89$ eV; $C_6H_5CF_3$: $IP_1 = -9.75$ eV [15]; C_6H_5Br: $IP_1 = -9.02$ eV; HC≡CH: $IP_1 = -11.4$ eV [16]; $Me_3SiSiMe_3$: $IP_1 = -8.69$ eV [1a]), the HOMO's in the whole series are best described by highly delocalized

Table 3
Experimental and calculated UV/vis data

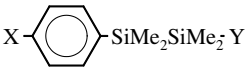

X	Y	λ_{max} exp.[a] (nm)	ε ($l\,mol^{-1}\,cm^{-1}$)	λ_{max} Calc.[b] *gauche*	λ_{max} Calc.[b] (nm) *trans*
Me_2N–	Me	270[c]	–[d]	–	–
Me_2N–	HC≡C–	271[e]	39 000	262.5 (HO → LU + 1)	265.4 (HO → LU + 1)
Me	Me	233[c]	–[d]	–	–
Me	HC≡C–	233	13 400	236 (HO → LU)	243 (HO → LU)
H	Me	231[c]	10 800	–	–
H	HC≡C–	233	13 900	235.2 (HO → LU)	239.5 (HO → LU)
Br	HC≡C–	239	13 800	245 (HO → LU)	249 (HO → LU)
F_3C–	Me	239.5[f]	6820	–	–
F_3C–	HC≡C–	239	6200	252 (HO → LU)	256 (HO → LU)

[a] C_6H_{12} solution, $c = 5 \times 10^{-5}$ mol · l^{-1}.
[b] Time-dependent DFT B3LYP/TZVP.
[c] Data taken from Ref. [4a].
[d] Not reported.
[e] Data taken from Ref. [4b].
[f] $c = 5 \times 10^{-6}$ mol l^{-1}.

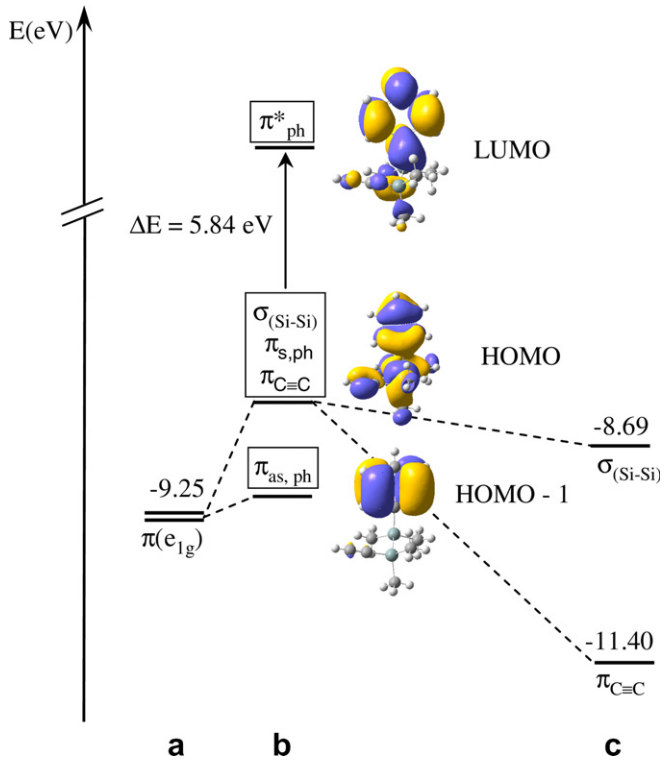

Fig. 5. Frontier orbital diagram for **2** (b). Energies of highest occupied MO's of (a) benzene and (c) hexamethyldisilane and acetylene are derived from PES measurements [17]. Orbital shapes were calculated using density functional theory (Gaussian 03; B3LYP/6-31+G**).

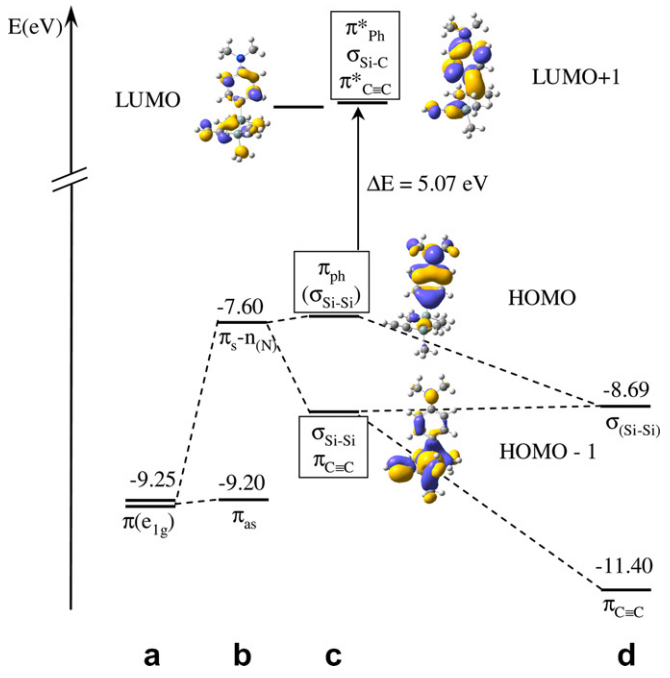

Fig. 6. Frontier orbital diagram for **1** (c). Energies of highest occupied MO's of (a) benzene, (b) *N*,*N*-dimethylaminobenzene and (d) hexamethyldisilane and acetylene are derived from PES measurements [17]. Orbital shapes were calculated using density functional theory (Gaussian 03; B3LYP/6-31+G**).

orbitals with a large σ(Si–Si) contribution and **2** may serve as a model substance for the understanding of the absorption behavior of **3**, **4** and **5** as well. This picture is perfectly in line with the computational results obtained for **3**–**5**, which are included in the Supplementary material. The low energy UV absorption bands observed for **2**–**5** between 233 and 239 nm, thus, can be assigned to σ(Si–Si) → π* electron transitions. The small difference of the excitation energies within the series **2**–**5** indicates only minor impact of the X-groups attached to the phenyl ring on the extent of σ–π conjugation.

The strong absorption maximum at 271 nm visible in the spectrum of **1** is characteristic for compounds containing the Me_2N–phenyl moiety. In *p*-sila-*N*,*N*-dimethylanilines it is usually found around 270 nm and can be assigned to a localized transition within the aromatic system with minor contributions of the *p*-silanyl substituent [17]. This model is fully supported by our computational results (compare Fig. 6) obtained for **1**. Due to the effective mixing of the *n*(*N*) and benzene π orbitals the highest occupied π–MO is raised above the σ(Si–Si) level, and the HOMO in **1** is primarily π in character with negligible σ(Si–Si) contribution. The 271 nm band in the absorption spectrum of **1** is assigned computationally to the HOMO → LUMO + 1 transition, where the electron is excited from this π(Ph) type HOMO to an orbital with $\pi^*_{ph}/\pi^*_{C\equiv C}/\sigma_{Si-C}$ character.

In the literature, contributions of several conformers are frequently invoked to explain the UV absorption spectra of polysilane chains and cycles [2d,18,19]. The *gauche* and the *anti* rotational isomers of **1**–**5**, however, were calculated to exhibit very similar absorption spectra. Combined with the low rotational barrier around the Si–Si bond calculated for **1** and **2** this result clearly rules out, that the differences in the absorption spectra of **1**–**5** arise from variable contributions of the *gauche* and the *anti* rotational isomers.

3. Conclusions

Experimental and computational results presented in this paper provide significant evidence for extended σ–π conjugation within the family of disilanes **1**–**5**. Experimental absorption spectra exhibit absorption maxima in the near UV, the position and intensity of which are influenced by the presence of electronically active substituents attached to the phenyl ring in para position. DFT calculations allow the assignment of the observed absorption bands to σ(Si–Si) → π*(ph) or π(ph) → π*(ph) electron transitions depending on the substituents attached to the benzene ring. Unusual structural features found for **1** experimentally by single crystal X-ray crystallography, however, are rather due to crystal packing and solid state effects than intramolecular electronic interactions, because they are much less pronounced in the calculated gas phase structure of the molecule. Currently attempts are made in our laboratories to link the terminal acetylene group in **1**–**5** to electron rich transition metal centers in order to study donor–acceptor substituent interactions via the silicon–silicon bond.

4. Experimental section

4.1. General procedures

Manipulations of air-sensitive compounds were performed under a nitrogen atmosphere using standard Schlenk techniques. Solvents were dried using a column solvent purification system [20]. *p*-Bromo-*N*,*N*-dimethylaniline, *p*-bromotoluene and 1-bromo-4-trifluoromethylbenzene (Aldrich, Acros) were purchased and used as obtained. $ClSiMe_2SiMe_2Cl$ [21], $ClMe_2SiSiMe_2PhBr$ [3a] and compound **2** [22] were prepared using published procedures. Reaction completion was verified with GC/MS on a HP 5890 II and HP 5971 with a 25 m long polydimethylsiloxane column. Infrared spectra were obtained as Nujol mulls or as films between KBr windows with a Bruker IFS28 FT-IR infrared spectrophotometer (4000–400 cm^{-1}). UV–visible spectra were recorded on a Perkin–Elmer Lambda 35 spectrometer. ^1H and ^{13}C NMR spectra were recorded on a Bruker DPX200, ^{29}Si NMR spectra were recorded on a Varian INOVA 300 MHz at room temperature. Chemical shifts are reported in parts per million (δ) relative to tetramethylsilane (TMS), using the residual solvent resonances as internal references. Coupling constants (J) are reported in hertz (Hz), and integrations are reported as numbers of protons. The following abbreviations are used alone or together to describe peak patterns: singlet = s, doublet = d, triplet = t, quartet = q, quintet = p, septet = h, m = multiplet. High-resolution mass spectra (HRMS) were recorded on a high-resolution VARIAN MAT 311 analytical spectrometer operating in the EI mode, at the Centre Régional de Mesures Physiques de l'Ouest (CRMPO), Rennes. Polyethyleneglycol (PEG) was used as internal reference, and methanol was used as solvent. All mass measurements refer to peaks for the most common isotopes (^1H, ^{12}C, ^{14}N, ^{19}F, ^{28}Si). Elemental analyses were conducted on a Thermo-FINNIGAN Flash EA 1112 CHNS/O analyzer by the Microanalytical Service of the CRMPO at the University of Rennes 1, France.

4.2. 1-(p-N,N-Dimethylaminophenyl)-2-chlorotetramethyldisilane

A solution of *p*-$Me_2NPhMgBr$ prepared from 2.15 g (88.46 mmol) of Mg and 15.0 g (0.075 mol) of *p*-Me_2NPhBr in 50 mL of THF was added at 0 °C to 13.9 g (0.075 mol) of $ClSiMe_2SiMe_2Cl$ dissolved in 100 mL of THF over a period of 2 h. After stirring the resulting solution at room temperature for 16 h the reaction was shown by GC/MS to have gone to completion. Work-up was achieved by evaporating the solvent and extracting the solid residue with a 50:1 mixture of toluene and THF. Upon removal of the solvents in vacuum, the desired product (10.2 g, 50%) appeared as a white air- and moisture-sensitive solid, which was used without further purification.

^1H NMR (THF/ext. lock D_2O, ext. TMS, ppm, rel. Int.): $\delta = 7.42$–6.81 (AA'BB', 4H, $C_6\mathbf{H}_4$); 3.01 (s, 6H, NMe_2); 0.46 (s, 6H, $SiMe_2Cl$); 0.44 (s, 6H, $SiMe_2$–C_{aryl}). ^{29}Si NMR (THF/ext. lock D_2O, ext. TMS, ppm): $\delta = 22.53$ (SiMe$_2$Cl); -22.79 (SiMe$_2$–C_{aryl}).

4.3. 1-(p-Trifluoromethylphenyl)-2-chlorotetramethyldisilane

The procedure followed was that used for the Me_2N-derivative as described above with 5.0 g (0.022 mol) of *p*-F_3CPhBr, 0.7 g (0.029 mol) Mg, 4.5 g (0.025 mol) of $ClSiMe_2SiMe_2Cl$ and 35 mL of THF. After the evaporation of THF, 4.9 g (74%) of the title compound were isolated from the crude product mixture by extraction with pentane. The slightly yellow, air- and moisture-sensitive liquid was used without further purification.

^1H NMR (C_6D_6, ext. TMS, ppm, rel. Int.): $\delta = 7.40$–7.25 (AA'BB', 4H, $C_6\mathbf{H}_4$); 0.25 (s, 6H, $SiMe_2Cl$); 0.23 (s, 6H, $SiMe_2C_{aryl}$). ^{29}Si NMR (THF/ext. lock D_2O, ext. TMS, ppm): $\delta = 21.34$ (SiMe$_2$Cl); -21.30 (SiMe$_2$–C_{aryl}).

4.4. 1-(p-N,N-Dimethylaminophenyl)-2-ethynyltetramethyldisilane (**1**)

A solution of HC≡CMgBr (36 mL, 0.5 M) in THF was added dropwise to 5.0 g (0.018 mol) of $Me_2NPhSiMe_2SiMe_2Cl$ dissolved in 25 mL of THF. After stirring the resulting solution at room temperature overnight GC/MS analysis revealed that the reaction had gone to completion. The solvent was evaporated and the resulting solid extracted three times with pentane. After removal of the pentane in vacuum the crude product was purified by distillation to yield a white solid that readily formed air- and moisture-stable crystals of pure **1** from a saturated pentane solution at −40 °C with a yield of 2.5 g (53%).

B.p. (0.08 mbar): 95 °C. Anal. Found: C, 63.55; H, 8.91; N 5.33%. Calc. for $C_{14}H_{23}NSi_2$: C, 64.30; H, 8.86; N 5.36%. FT-IR (Nujol, cm^{-1}): 2022 (s) ν(C≡C). ^1H NMR ($CDCl_3$, ext. TMS, ppm, rel. Int.): $\delta = 7.47$–6.83 (AA'BB', 4H, $C_6\mathbf{H}_4$); 3.04 (s, 6H, NMe); 2.56 (s, 1H, C≡CH); 0.47 (s, 6H, $SiMe_2$); 0.30 (s, 6H, $SiMe_2$). ^{13}C NMR ($CDCl_3$, ext. TMS, ppm): 150.9 (s, C_4Ar); 135.1 (dd, $^1J_{C-H} = 155.4$ Hz, C_2Ar); 122.6 (s, C_1Ar); 112.2 (dd, $^1J_{C-H} = 157.2$ Hz, C_3Ar); 95.3 (dh, $^1J_{C-H} = 236.43$ Hz, $^4J_{C-H} = 3.3$ Hz, C≡CH); 89.5 (d, $^2J_{C-H} = 41.7$ Hz, C≡CH); 40.3 (qq, $^1J_{C-H} = 135.2$ Hz, $^4J_{C-H} = 3.8$ Hz, NMe); −2.85 (qq, $^1J_{C-H} = 121.6$ Hz, $^4J_{C-H} = 2.2$ Hz, $SiMe_2$); −3.8 (qq, $^1J_{C-H} = 120.7$ Hz, $^4J_{C-H} = 2.4$ Hz, $SiMe_2$). ^{29}Si NMR (THF/ext. lock D_2O, ext. TMS, ppm): $\delta = -23.16$ (SiMe$_2$–C_{sp2}); -37.10 (SiMe$_2$–C_{sp}). HRMS ($C_{14}H_{23}NSi_2$, [M^+]): 261.1369 (calc.); 261.1362 (found).

4.5. 1-(p-Tolyl)-2-ethynyltetramethyldisilane (**3**)

The synthesis of **3** was carried out in a one-pot fashion starting from *p*-bromotoluene and $ClSiMe_2SiMe_2Cl$. A solution of *p*-tolylMgBr prepared from 1.6 g (0.065 mol)

of Mg and 10.9 g (0.064 mol) of *p*-bromotoluene in 50 mL of THF was added at 0 °C to 11.9 g (0.064 mol) of $ClSiMe_2SiMe_2Cl$ dissolved in 100 mL of THF over a period of 2 h. After stirring the resulting solution at room temperature for 16 h the reaction was shown by GC/MS to have gone to completion. After dropwise addition of 130 mL of a 0.5 M solution of HC≡CMgBr in THF, the resulting mixture was stirred at room temperature overnight to achieve complete conversion (GC/MS monitoring recommended). After aqueous workup with 1 M H_2SO_4 and extraction with pentane, the combined organic layers were dried over Na_2SO_4. Removal of the solvent and fractional distillation of the liquid residue gave 10.9 g (74%) of pure **3** as a colorless oily liquid.

B.p. (0.03 mbar): 58–60 °C. FT-IR (Nujol, cm^{-1}): 2028 (s) *ν*(C≡C). ^1H NMR ($CDCl_3$, ext. TMS, ppm, rel. Int.): $\delta = 7.59$–7.34 (AA'BB', 4H, $C_6\mathbf{H}_4$); 2.62 (s, 1H, C≡C*H*); 2.51 (s, 3H, Aryl-*Me*); 0.59 (s, 6H, Si*Me*$_2$); 0.39 (s, 6H, Si*Me*$_2$). ^{13}C NMR ($CDCl_3$, ext. TMS, ppm): $\delta = 138.6$ (q, $^2J_{C-H} = 6.5$ Hz, C_4Ar); 134.2 (s, C_1Ar); 134.1 (dd, $^1J_{C-H} = 157.2$ Hz, C_2Ar); 128.8 (dm, $^1J_{C-H} = 157.2$ Hz, C_3Ar); 95.60 (d, $^1J_{C-H} = 237$ Hz, C≡*C*H); 88.97 (dm, $^2J_{C-H} = 41.9$ Hz, $^3J_{C-H} = 3.3$ Hz, *C*≡CH); 21.6 (qt, $^1J_{C-H} = 126.3$ Hz, $^3J_{C-H} = 4.5$ Hz, Ar*Me*); −2.9 (qq, $^1J_{C-H} = 121.7$ Hz, $^4J_{C-H} = 2.3$ Hz, Si*Me*$_2$); −4.0 (qq, $^1J_{C-H} = 121.0$ Hz, $^4J_{C-H} = 2.4$ Hz, Si*Me*$_2$). ^{29}Si NMR (THF/ext. lock D_2O, ext. TMS, ppm): $\delta = -22.26$ (*Si*Me$_2$–C$_{sp2}$); −36.78 (*Si*Me$_2$–C$_{sp}$). HRMS ($C_{13}H_{20}Si_2$, [M^+]): 232.1104 (calc.); 232.1112 (found).

4.6. 1-(p-Bromophenyl)-2-ethynyltetramethyldisilane (4)

The procedure followed was that used for **1** with 3.5 g (0.011 mol) of $BrPhSiMe_2SiMe_2Cl$, 28 mL of 0.5 M HC≡CMgBr in THF and 15 mL of THF. Fractional distillation of the crude product gave 3.0 g (86%) of pure **4** as a colorless air- and moisture-stable liquid.

B.p. (0.03 mbar): 75 °C. FT-IR (Nujol, cm^{-1}): 2028 (s) *ν*(C≡C). ^1H NMR ($CDCl_3$, ext. TMS, ppm, rel. Int.): $\delta = 7.56$–7.44 (AA'BB', 4H, $C_6\mathbf{H}_4$); 2.55 (s, 1H, C≡C*H*); 0.49 (s, 6H, Si*Me*$_2$); 0.28 (s, 6H, Si*Me*$_2$). ^{13}C NMR ($CDCl_3$, ext. TMS, ppm): $\delta = 136.9$ (s, C_4Ar); 135.5 (dd, $^1J_{C-H} = 160$ Hz, C_2Ar); 131.0 (dd, $^1J_{C-H} = 167$ Hz, C_3Ar); 125.7 (s, C_1Ar); 95.9 (d, $^1J_{C-H} = 237$ Hz, C≡*C*H); 88.5 (dm, $^2J_{C-H} = 42.0$ Hz, $^3J_{C-H} = 3.3$ Hz, *C*≡CH); −2.30 (qq, $^1J_{C-H} = 122$ Hz, $^4J_{C-H} = 2.3$ Hz, Si*Me*$_2$); −3.49 (qq, $^1J_{C-H} = 121$ Hz, $^4J_{C-H} = 2.4$ Hz, Si*Me*$_2$). ^{29}Si NMR (THF/ext. lock D_2O, ext. TMS, ppm): $\delta = -21.12$ (*Si*Me$_2$–C$_{sp2}$); −36.67 (*Si*Me$_2$–C$_{sp}$). HRMS ($C_{12}H_{17}BrSi_2$, [M^+]): 296.00522 (calc.); 296.031 (found).

4.7. 1-(p-Trifluoromethylphenyl)-2-ethynyltetramethyldisilane (5)

The procedure followed was that used for **1** with 7.4 g (0.025 mol) of $F_3CPhSiMe_2SiMe_2Cl$, 60 mL of 0.5 M HC≡CMgBr in THF and 15 mL of diethyl ether. Fractional distillation of the crude product gave 5.6 g (79%) of pure **5** as a colorless air- and moisture-stable liquid.

B.p. (0.03 mbar): 46 °C. FT-IR (Nujol, cm^{-1}): 2029 (s) *ν*(C≡C). ^1H NMR ($CDCl_3$, ext. TMS, ppm, rel. Int.): $\delta = 7.85$–7.75 (AA'BB', 4H, $C_6\mathbf{H}_4$); 2.55 (s, 1H, C≡C*H*); 0.51 (s, 6H, Si*Me*$_2$); 0.28 (s, 6H, Si*Me*$_2$). ^{13}C NMR ($CDCl_3$, ext. TMS, ppm): $\delta = 143.5$ (s, C_1Ar); 134.3 (dd, $^1J_{C-H} = 160.7$ Hz, C_2Ar); 127.2 (m, C_1Ar); 130.9 (qt, $^1J_{C-F} = 128.0$ Hz, *C*F$_3$); 124.8 (dm, $^1J_{C-H} = 160.7$ Hz, C_3Ar); 96.0 (d, $^1J_{C-H} = 237.3$ Hz, C≡*C*H); 88.3 (dm, $^2J_{C-H} = 45.5$ Hz, $^3J_{C-H} = 3.3$ Hz, *C*≡CH); -3.1 (qq, $^1J_{C-H} = 121.9$ Hz, $^4J_{C-H} = 2.4$ Hz, Si*Me*$_2$); −4.35 (qq, $^1J_{C-H} = 121.2$ Hz, $^4J_{C-H} = 2.5$ Hz, Si*Me*$_2$). ^{29}Si NMR (THF/ext. lock D_2O, ext. TMS, ppm): $\delta = -22.28$ (*Si*Me$_2$–C$_{sp2}$); −37.77 (*Si*Me$_2$–C$_{sp}$). HRMS ($C_{13}H_{17}F_3Si_2$, [M^+]): 286.0821 (calc.); 286.0823 (found).

4.8. X-ray crystallography

Single crystals suitable for X-ray crystallography of **1** were obtained as described above, and were mounted with epoxy cement on the tip of a glass fiber. Crystal, data collection, and refinement parameters are given in Table 4.

The compound was studied on a Kappa-CCD Enraf-Nonius FR590 diffractometer equipped with a bidimen-

Table 4
Crystallographic data for compound **1**

Empirical formula	$C_{14}H_{23}NSi_2$
Formula weight	261.51
Collection temperature (K)	173(2)
Crystal system	Monoclinic
Crystal size (mm)	$0.7 \times 0.4 \times 0.12$
Space group	$P2_1/a$
a (Å)	12.3423(5)
b (Å)	8.2962(4)
c (Å)	16.4090(7)
α (°)	90.00
β (°)	108.405(2)
γ (°)	90.00
Volume (Å^3)	1594
Z	4
Absorption coefficient (mm^{-1})	0.204
Density calc. (g cm^{-3})	1.090
F(000)	568
θ Range (°)	2.72–27.52
Limiting indices	$-16 < h < 9$, $-10 < k < 10$, $-20 < l < 20$
Reflections collected	21 163
Independent reflections	3654
Completeness to $\theta = 27.52°$	99.8%
Max. and min. transmission	0.976 and 0.867
Data/restraints/parameters	3654/0/154
Final *R* indices [$I > 2\sigma(I)$]	$R_1 = 0.0264$, $wR_2 = 0.0759$
R indices (all data)	$R_1 = 0.0290$, $wR_2 = 0.0779$
Goodness-of-fit on F^2	1.039
Largest difference in peak and hole (e Å^{-3})	0.349 and −0.180

sional CCD detector employing graphite-monochromated Mo K_α radiation ($\lambda = 0.71073$ Å). The cell parameters were obtained with Denzo and Scalepack with 10 frames (psi rotation: 1° per frame) [23]. The data collection provided 21 163 reflections (Table 4). Subsequent data reduction with Denzo and Scalepack gave the independent reflections (Table 4). The space group was chosen based on the systematic absences in the diffraction data. The structure was solved with SIR-97 which revealed the non-hydrogen atoms [24]. After anisotropic refinement, the remaining atoms were found in Fourier difference maps. The complete structure was then refined with SHELXL97 by the full-matrix least-squares procedures on reflection intensities (F^2) [25]. The absorption was not corrected. The non-hydrogen atoms were refined with anisotropic displacement coefficients, and all hydrogen atoms were treated as idealized contributions. Atomic scattering factors were taken from the literature [26].

4.9. Computational methods

Geometry optimizations and analytical vibrational frequency calculations were carried out with the Gaussian 03 program suite [27] at the density functional level using the B3LYP hybrid functional and 6-31+G** basis sets as implemented. The UV spectra obtained by time-dependent B3LYP/TZVP calculations were performed with the Turbomole V5.6 program [28]. Relative energies given include zero point vibrational energy (ZPVE) corrections.

Acknowledgements

The authors are grateful to Drs P. Jehan and P. Guénot (CRMPO, Rennes) for skillful assistance in recording high-resolution mass spectra. Financial support from the Austrian-French scientific exchange program (AMADEUS 20/2004-05), the Centre National de la Recherche Scientifique (CNRS), the Technische Universität Graz, the Université de Rennes 1, and the Ministère de l'Education Nationale de l'Enseignement Supérieur et de la Recherche (MENESR, Grant for J.S.-T.) is gratefully acknowledged. We wish to thank the WACKER CHEMIE GMBH (Burghausen, Germany) for the donation of silane precursors.

Appendix A. Supplementary material

CCDC 613923 contains the supplementary crystallographic data for **1**. These data can be obtained free of charge via http://www.ccdc.cam.ac.uk/conts/retrieving.html, or from the Cambridge Crystallographic Data Centre, 12 Union Road, Cambridge CB2 1EZ, UK; fax: (+44) 1223-336-033; or e-mail: deposit@ccdc.cam.ac.uk. Supplementary data associated with this article can be found, in the online version, at doi:10.1016/j.jorganchem.2007.01.024.

References

[1] (a) C.G. Pitt, H. Bock, J. Chem. Soc., Chem. Commun. (1972) 28;
(b) C.G. Pitt, R.N. Carey, E.C. Toren, J. Am. Chem. Soc. 94 (1972) 3806.
[2] (a) For some reviews concerning the electronic properties of polysilanes, consult: C.G. Pitt, in: A.L. Rheingold (Ed.), Homoatomic Rings, Chains and Macromolecules of Main Group Elements, Elsevier, New York, 1977, p. 203;
(b) H. Sakurai, J. Organomet. Chem. 200 (1980) 261;
(c) H. Sakurai, Pure Appl. Chem. 59 (1987) 1637;
(d) R.D. Miller, J. Michl, Chem. Rev. 89 (1989) 1359;
(e) R. West, in: G. Wilkinson, F.G.A. Stone, E.W. Abel (Eds.), Comp. Organomet. Chem. II, vol. 2, Pergamon Press, 1995, p. 77;
(f) E. Hengge, H. Stueger, in: S. Patai, Z. Rappoport, Y. Apeloig (Eds.), The Chemistry of Organic Silicon Compounds, vol. 2, Wiley, Chichester, 1998, p. 2177.
[3] (a) G. Mignani, M. Barzoukas, J. Zyss, G. Soula, F. Balegroune, D. Grandjean, D. Josse, Organometallics 10 (1991) 3660;
(b) D. Hissink, P.F. van Hutten, G. Hadziioannou, J. Organomet. Chem. 454 (1993) 25;
(c) H.K. Sharma, K.H. Pannell, I. Ledoux, J. Zyss, A. Ceccanti, P. Zanello, Organometallics 19 (2000) 770;
(d) C. Grogger, H. Rautz, H. Stueger, Mh. Chem. 132 (2001) 453.
[4] (a) H. Sakurai, H. Sugiyama, M. Kira, J. Phys. Chem. 94 (1990) 1837;
(b) M. Kira, T. Miyazawa, H. Sugiyama, M. Yamaguchi, H. Sakurai, J. Am. Chem. Soc. 115 (1993) 3116;
(c) M. Yamamoto, T. Kudo, M. Ishikawa, S. Tobita, H. Shizuka, J. Phys. Chem. A 103 (1999) 3144.
[5] For reviews consult Ref. [2a,2d] and H.A. Fogarty, D.L. Casher, R. Imhof, T. Schepers, D.W. Rooklin, J. Michl, Pure Appl. Chem. 75 (2003) 999.
[6] (a) D.N. Hague, R.H. Prince, J. Chem. Soc. (1965) 4690;
(b) H. Gilman, W.H. Atwell, G.L. Schwebke, J. Organomet. Chem. 2 (1964) 369;
(c) H. Sakurai, S. Tasaka, M. Kira, J. Am. Chem. Soc. 94 (1972) 9285;
(d) C.G. Pitt, J. Am. Chem. Soc. 91 (1969) 6613;
(e) H. Stueger, E. Hengge, Mh. Chem. 119 (1988) 873;
(f) H. Stueger, G. Fuerpass, K. Renger, Organometallics 24 (2005) 6374.
[7] H. Sakurai, M. Kira, T. Uchida, J. Am. Chem. Soc. 95 (1973) 6826.
[8] (a) R. West, in: Z. Rappoport, Y. Apeloig (Eds.), The Chemistry of Organic Silicon Compounds, vol. 3, Wiley, Chichester, 2001, p. 541;
(b) H. Tsuji, J. Michl, K. Tamao, J. Organomet. Chem. 685 (2003) 9.
[9] M. Kira, T. Miyazawa, N. Mikami, H. Sakurai, Organometallics 10 (1991) 3793.
[10] (a) K. Tamao, H. Tsuji, M. Terrada, M. Asahara, S. Yamaguchi, A. Toshimitsu, Angew. Chem. 112 (2000) 3425;
(b) H. Tsuji, Y. Shibano, T. Takahashi, M. Kumada, K. Tamao, Bull. Chem. Soc. Jpn. 78 (2005) 1334.
[11] (a) E.A. Williams, J.D. Cargioli, P.E. Donahue, J. Organomet. Chem. 192 (1979) 319;
(b) E.R.H. Jones, L. Skatterbol, M.C. Whiting, J. Chem. Soc. (1956) 4765.
[12] (a) D.F. Ewing, Org. Magn. Res. 12 (1979) 499;
(b) E. Breitmaier, W. Voelter, Carbon-13 NMR Spectroscopy, third ed., VCH, Weinheim, 1987, p. 259.
[13] (a) C. Grogger, H. Fallmann, G. Fuerpass, H. Stueger, G. Kickelbick, J. Organomet. Chem. 665 (2003) 186;
(b) H. Stueger, M. Braunwarth, G. Fuerpass, J. Baumgartner, R. Saf, Mh. Chem. 137 (2006) 595.
[14] G. Mignani, A. Krämer, G. Pucetti, I. Ledoux, G. Soula, J. Zyss, Mol. Eng. 1 (1991) 11.
[15] B.G. Ramsey, J. Organomet. Chem. 135 (1977) 307.

[16] V.F. Traven, Frontier Orbitals and Properties of Organic Molecules, Ellis Horwood, New York, 1992.
[17] (a) D. Hissink, H. Bolink, J.W. Eshuis, G.G. Malliaras, G. Hadziioannou, Polym. Prepr. 34 (1993) 721;
(b) G. Hadziioannou, J. Wildeman, J. Herrema, P. Soeteman, D. Hissink, J. Brouwer, R. Flipse, Polym. Prepr. 32 (1991) 90;
(c) P.F. vanHutten, G. Hadziioannou, R. Bursi, D. Feil, J. Phys. Chem. 100 (1996) 85.
[18] H.S. Plitt, V. Balaji, J. Michl, Chem. Phys. Lett. 213 (1993) 158.
[19] Recently we were able to show, that different conformers contribute to the UV absorption spectra of cyclohexasilane derivatives $Si_6Me_{6-n}X_n$: H. Stueger, G. Fuerpass, M. Flock, Lecture presented at the 38th Organosilicon Symposium, Boulder CO, USA, 2–5 June, 2005.
[20] A.B. Pangborn, M.A. Giardello, R.H. Grubbs, R.K. Rosen, F.J. Timmers, Organometallics 15 (1996) 1518.
[21] M. Ishikawa, M. Kumada, H. Sakurai, J. Organomet. Chem. 23 (1970) 63.
[22] M. Ishikawa, H. Sugisawa, K. Yamamoto, M. Kumada, J. Organomet. Chem. 179 (1979) 377.
[23] Nonius Kappa CCD Software, Nonius B.V., Delft, Netherlands, 1999.
[24] M.C. Altomare, M. Burla, G. Camalli, C. Cascarano, A. Giacovazzo, A.G.G. Guagliardi, G. Moliterni, R. Polidori, R. Spagna, J. Appl. Crystallogr. 31 (1998) 74.
[25] G.M. Sheldrick, SHELX97. Program for the Refinement of Crystal Structures, University of Göttingen, Göttingen, Germany, 1997.
[26] A.J.C. Wilson (Ed.), International Tables for X-ray Crystallography, vol. C, Kluwer Academic Publishers., Dordrecht, The Netherlands, 1992.
[27] M.J. Frisch, G.W. Trucks, H.B. Schlegel, G.E. Scuseria, M.A. Robb, J.R. Cheeseman, J.A. Montgomery Jr., T. Vreven, K.N. Kudin, J.C. Burant, J.M. Millam, S.S. Iyengar, J. Tomasi, V. Barone, B. Mennucci, M. Cossi, G. Scalmani, N. Rega, G.A. Petersson, H. Nakatsuji, M. Hada, M. Ehara, K. Toyota, R. Fukuda, J. Hasegawa, M. Ishida, T. Nakajima, Y. Honda, O. Kitao, H. Nakai, M. Klene, X. Li, J.E. Knox, H.P. Hratchian, J.B. Cross, C. Adamo, J. Jaramillo, R. Gomperts, R.E. Stratmann, O. Yazyev, A.J. Austin, R. Cammi, C. Pomelli, J.W. Ochterski, P.Y. Ayala, K. Morokuma, G.A. Voth, P. Salvador, J.J. Dannenberg, V.G. Zakrzewski, S. Dapprich, A.D. Daniels, M.C. Strain, O. Farkas, D.K. Malick, A.D. Rabuck, K. Raghavachari, J.B. Foresman, J.V. Ortiz, Q. Cui, A.G. Baboul, S. Clifford, J. Cioslowski, B.B. Stefanov, G. Liu, A. Liashenko, P. Piskorz, I. Komaromi, R.L. Martin, D.J. Fox, T. Keith, M.A. Al-Laham, C.Y. Peng, A. Nanayakkara, M. Challacombe, P.M.W. Gill, B. Johnson, W. Chen, M.W. Wong, C. Gonzalez, J.A. Pople, Gaussian 03, Rev. C.02, Gaussian, Inc., Wallingford CT, 2004.
[28] R. Ahlrichs, M. Baer, H.P. Baron, R. Bauernschmitt, S. Boecker, M. Ehrig, K. Eichkorn, S. Elliott, F. Furche, F. Haase, M. Haeser, H. Horn, C. Huber, U. Huniar, M. Kattannek, C. Koelmel, M. Kollwitz, K. May, C. Ochsenfeld, H. Oehm, A. Schaefer, U. Schneider, O. Treutler, M. von Arnim, F. Weigend, P. Weis, H. Weiss, TURBOMOLE (Vers. 5.6), Universitaet Karlsruhe, 2002.